Journal of Materials Chemistry A

Accepted Manuscript

ROYAL SOCIETY OF CHEMISTRY

www.rsc.org/materialsA

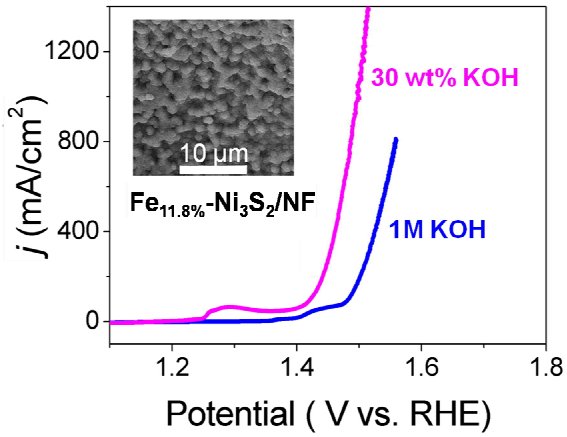

Fe-doped Ni_3S_2 particles film grown on nickel form ($Fe_{11.8\%}$-Ni_3S_2/NF) behaves as a high-efficiency and robust oxygen evolution electrode in strongly alkaline solution.

Journal Name

ARTICLE

Fe-doped Ni_3S_2 particles film as a high-efficiency robust oxygen evolution electrode with very high current density

Received 00th January 20xx,
Accepted 00th January 20xx

Ningyan Cheng,[a,b] Qian Liu,[a] Abdullah M. Asiri,[c] Wei Xing[d] and Xuping Sun[a*]

DOI: 10.1039/x0xx00000x

www.rsc.org/

The efficiency of water splitting is mainly limited by the low rate of oxygen evolution reaction (OER) and it is thus of great importance but still remains a huge challenge to develop efficient OER catalysts capable of delivering high current densities at low overpotentials. Herein, we describe our recent finding that Fe-doped Ni_3S_2 particles film with 11.8% Fe-content hydrothermally grown on nickel foam ($Fe_{11.8\%}$-Ni_3S_2/NF) behaves as a high-active robust oxygen evolution electrode in strongly alkaline media. This electrode needs overpotential of only 253 mV to achieve 100 mA/cm^2 with a Tafel slope of 65.5 mV/dec and maintains its catalytic activity for at least 14 h in 1 M KOH, and the NiOOH and FeOOH formed at the $Fe_{11.8\%}$-Ni_3S_2 surface are the actual catalytic sites. Notably, it also operates efficiently and stably in 30 wt% KOH, capable of affording very high current densities of 500 and 1,000 mA/cm^2 at small overpotentials of 238 and 269 mV, respectively, with Faradaic efficiency of 100%.

Introduction,

The growing depletion of non-renewable resources and the increasing concerns about environment pollution from fossil fuels have stimulated intense interest in energy conversion and storage from alternative sustainable energy sources.[1] Hydrogen is considered as an ideal clean fuel essential to several key industrial processes and could play a major role as an energy carrier in a future hydrogen economy.[2] Splitting of water affords a promising solution to hydrogen generation from renewable energy sources like solar and wind power,[3,4] but the sluggish kinetics of the oxygen evolution reaction (OER) proceeding through several steps with high activation energies severely limits the efficiency of hydrogen production.[5,6] Thus, efficient OER catalysts must be utilized to accelerate the reaction rate and reduce the overpotential.[4] The best OER catalysts (IrO_2 and RuO_2) suffer from scarcity and high cost hampering their widespread use,[7] which pushes the development of efficient, earth-abundant alternatives.

Ni has emerged as an interesting non-precious metal for its catalytic power toward oxygen evolution and considerable recent research attention has been paid to make Ni-based inorganic materials as active OER catalysts, including oxides/hydroxides,[8-11] chalcogenides,[12,13] and nitrides[14,15] etc, and some Ni-containing mixed-metal oxides/hydroxides[11,16-24] and sulfide[25,26] has also been developed. It has also been reported that heterogeneous metal doping leads to enhanced OER activity of Ni-based oxides/hydroxides.[27-29] Although with such great success, these catalysts cannot satisfy the requirements for industrial applications where very high current densities (≥ 500 mA/cm^2) are driven at low overpotentials (≤ 300 mV). Only until recently have Lu *et al.* reported electrodeposition of hierarchically structured three-dimensional NiFe double hydroxide on nickel foam (NiFe/NF) as an efficient oxygen evolution electrode which needs overpotential of 270 mV to drive 1,000 mA/cm^2 in 10 M KOH.[30]

The superior electronic conductivity of most sulfides to oxides/hydroxides[31] offers a great benefit to electrochemical performance of catalysts. Fe-doped nickel sulfide is thus expected to work as a high-performance OER catalyst, which, however, has not been explored before. In this work, we describe our recent finding that Fe-doped Ni_3S_2 particles film in situ hydrothermally grown on NF with 11.8% Fe-content ($Fe_{11.8\%}$-Ni_3S_2/NF) behaves as a cost-effective OER electrode excellent in activity and stability in strongly alkaline electrolytes. This electrode affords 100 mA/cm^2 at overpotential (η) of only 253 mV with a Tafel slope of 65.5 mV/dec in 1 M KOH. Remarkably, it still maintains strong long-term electrochemical durability with superior activity in 30 wt% KOH, requiring small overpotentials of 238 and 269 mV to drive very high current densities of 500 and 1,000 mA/cm^2, respectively, with 100% Faradaic efficiency (FE).

Experimental

[a] *State Key Laboratory of Electroanalytical Chemistry, Changchun Institute of Applied Chemistry, Chinese Academy of Sciences, Changchun 130022, Jilin, China. E-mail: sunxp@ciac.ac.cn*
[b] *University of the Chinese Academy of Sciences, Beijing 100049, China*
[c] *Chemistry Department & Center of Excellence for Advanced Materials Research, King Abdulaziz University, Jeddah 21589, Saudi Arabia*
[d] *Laboratory of Advanced Power Sources, Changchun Institute of Applied Chemistry, Chinese Academy of Sciences, Changchun 130022, Jilin, China*

Electronic Supplementary Information (ESI) available: [EDX spectrum, XPS spectra, XRD patterns, SEM images, Polarization curve, CVs and Raman spectra]. See DOI: 10.1039/x0xx00000x

Materials

$FeSO_4 \cdot 7H_2O$ and KOH were purchased from Beijing Chemical Corp. Nickel foam (NF) was purchased from Shenzhen Green and Creative Environmental Science and Technology Co. Ltd. Ethanol was purchased from Aladdin Ltd. (Shanghai, China). Pt/C (20 wt% Pt on Vulcan XC-72R) and Nafion (5 wt%) were purchased from Sigma-Aldrich. All the reagents were used as received. The water used throughout all experiments was purified through a Millipore system.

Preparation of $Fe_{x\%}$-Ni_3S_2/NF and Ni_3S_2/NF

$Fe_{11.8\%}$-Ni_3S_2/NF was prepared as follows. Typically, 1.75 mmol of $FeSO_4 \cdot 7H_2O$ and 5.25 mmol of L-cysteine were dissolved in 35 mL water under stirring for 1 h. Then the solution was transferred into a Teflon-lined stainless autoclave (50 mL) and a piece of NF (2.5 cm × 3.5 cm), which was cleaned by sonication sequentially in acetone, ethanol and water for 30 min each, was immersed into the solution. The autoclave was sealed and maintained at 150 °C for 10 h in electric oven. After the autoclave cooled down slowly at room temperature, the NF was taken out and washed with water thoroughly before vacuum dried. $Fe_{6.5\%}$-Ni_3S_2/NF and $Fe_{14.9\%}$-Ni_3S_2/NF were prepared similarly by adjusting the amount of $FeSO_4 \cdot 7H_2O$ to 0.875 mmol and 2.625 mmol, respectively. Ni_3S_2/NF was made without the addition of $FeSO_4 \cdot 7H_2O$. The Fe-content was calculated using the equation: Fe (wt)% = [Mr(Fe)]/[Mr(Fe) + 0.5 * n * Mr(Ni_3S_2)]. The mass loading of $Fe_{x\%}$-Ni_3S_2 grown on the NF was calculated as following: $m_{Fex\%\text{-}Ni3S2}$ = [Mr(Fe)]/[Mr(Fe) + n * Mr(S)] * y + [n * Mr(S)]/[Mr(Fe) + n * Mr(S)] * [Mr(Ni_3S_2)/2Mr(S)] * y. For Ni_3S_2/NF the mass loading of Ni_3S_2 grown on the NF was calculated as following: m_{Ni3S2} = [Mr(Ni_3S_2)/2Mr(S)] * y with Mr being the relative formula mass, n being the molar ratio of S to Fe obtained from the energy-dispersive X-ray spectra, and the weight increment (y mg) of Ni foam was directly weighted after the synthesis of on NF.

Preparation of RuO_2

RuO_2 catalyst was prepared as follows. In brief, 0.01 mol of $RuCl_3 \cdot 3H_2O$ was dissolved in 100 mL deionized water and heated under air atmosphere at 100°C for 10 min, followed by the addition of 1 mL KOH solution (1.0 M). The reaction mixture was maintained at this temperature under stirring for 45 min. After that, the solution was centrifuged for 10 minutes and filtered. The precipitate was washed several times with deionized water to remove the remaining chlorides. The resulting Ru-hydroxide was dried for 5 h at 80°C and then calcined in air at 300°C for 3 h to obtain RuO_2.

Characterizations

Powder XRD data were collected on Bruker D8 ADVANCE Diffractiometer (λ=1.5418 Å). XPS analysis was carried out on a Thermal ESCALAB 250 spectrometer using an Al Kα X-ray source (1486.6 eV photons). SEM measurements were performed on a XL30 ESEM FEG scanning electron microscope at an accelerating voltage of 20 kV. TEM measurements were performed on a HITACHI H-8100 electron microscopy (Hitachi, Tokyo, Japan) with an accelerating voltage of 200 kV. GC analysis was carried out on GC–2014C (Shimadzu Co.) with thermal conductivity detector and nitrogen carrier gas. Pressure data during electrolysis were recorded using a CEM DT-8890 Differential Air Pressure Gauge Manometer Data Logger Meter Tester with a sampling interval of 1 point per second.

Electrochemical measurements

Electrochemical measurements are performed with a CHI 660D electrochemical analyzer (CH Instruments, Inc., Shanghai) in a standard three-electrode system using $Fe_{11.8\%}$-Ni_3S_2/NF as the working electrode, a graphite plate as the counter electrode and an Ag/AgCl electrode as the reference electrode. To prepare RuO_2 loaded electrodes, 20 mg RuO_2 and 10 μL 5 wt% Nafion solutions were dispersed in 1 mL 1:1 v water/ethanol solvent by 30 min sonication to form an ink finally. Then 98.7 μL catalyst ink was loaded on a TiM with a catalyst loading of 7.9 mg/cm^2. All electrolytes were saturated by oxygen bubbles before and during the experiments. Polarization curves were recorded using linear sweep voltammetry without the involvement of any activation process. Prior to measurement, resistance tests were made using the CHI software at corresponding open-circuit potentials (in the frequency range of 100 kHz–0.1 Hz) in the alkaline standard three-electrode system. All potentials measured were calibrated to RHE using the following equation: E (RHE) = E (Ag/AgCl) + 0.197 V + 0.059 * pH – iR.

Results and discussion

The energy-dispersive X-ray (EDX) spectrum of hydrothermally treated NF (Fig. S1) indicates the existence of Fe, Ni, and S elements while the X-ray powder diffraction (XRD) pattern (Fig. 1a) only shows diffraction peaks indexed to the (101), (110), (003), (113), and (122) planes for Ni_3S_2 (JCPDS 44-1418) with the observation of another two strong peaks arising from the substrate (JCPDS 65-2865). These observations suggest the formation of Fe-doped Ni_3S_2 with 11.8% Fe-content (see Experimental Section for calculation detail) and the resulting electrode is denoted as $Fe_{11.8\%}$-Ni_3S_2/NF. The scanning electron microscopy (SEM) images (Fig. 1b) demonstrate the full coverage of the surface of NF by $Fe_{11.8\%}$-Ni_3S_2 particles. Transmission electron microscopy (TEM) image (Fig. 1c) reveals the particles have diameters in the range of 400-800 nm. The high-resolution TEM (HRTEM) image (Fig. 1c inset) shows clear lattice fringes with an interplane distance of 0.184 nm corresponding to the (113) plane of Ni_3S_2 phase. Fig. 1d presents the SEM and corresponding EDX elemental mapping images of Fe, Ni, and S for $Fe_{11.8\%}$-Ni_3S_2/NF, suggesting the uniform distribution of Fe, Ni, and S elements. The X-ray photoelectron spectroscopy (XPS) spectrum in Ni 2p region (Fig. 1e) shows two strong peaks at 856.2 and 874.2 eV, corresponding to the Ni $2p_{3/2}$ and Ni $2p_{1/2}$ of, respectively.[12,32]

The peak at 852.8 eV can be attributed to Ni_3S_2 or nickel.[12,33] The satellite peaks at 861.8 and 879.8 eV are shakeup type peaks of nickel.[34] The two peaks at 711.9 and 725.1 eV in Fe 2p region (Fig. 1f) correspond to Fe $2p_{3/2}$ and Fe $2p_{1/2}$, respectively, indicating the presence of Fe(III).[35] The absence of satellite peaks of Fe_2O_3 at around 719 and 732 eV excludes the existence of Fe_2O_3.[36] The peaks at 161.5 eV and 162.8 eV in the S 2p region (Fig. S2a) correspond to the S $2p_{3/2}$ and S $2p_{1/2}$, respectively, attributing to the S^{2-} of Ni_3S_2.[37] The additional peak at 168.8 eV is typical for Ni-O-S species with high oxidation state of sulfur, which is due to the surface oxidation in air.[37] The peak at 531.2 eV in O 1s region (Fig. S2b) corresponds to NiO generated by the surface oxidation.32 The other peak at 532.7 eV may be due to absorbed water or possibly adsorbed O_2.[33] All the results confirm the incorporation of Fe(III) into the Ni_3S_2 lattice. Note that the same preparation without the presence of Fe salt produces Ni_3S_2 particles film on NF (Ni_3S_2/NF), as shown in Fig. S3.

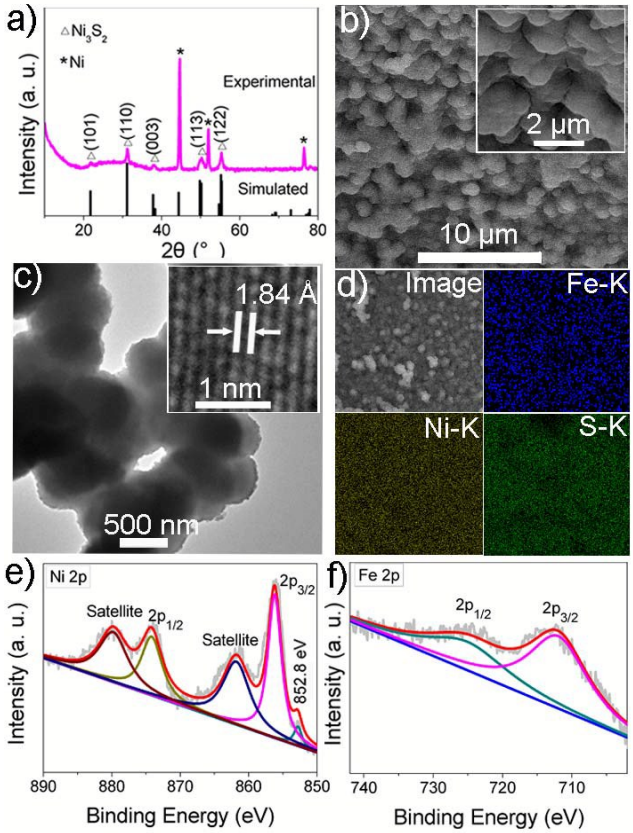

Fig. 1 (a) XRD pattern of $Fe_{11.8\%}$-Ni_3S_2/NF. (b) SEM images of $Fe_{11.8\%}$-Ni_3S_2/NF. (c) TEM and HRTEM (inset) images of $Fe_{11.8\%}$-Ni_3S_2 particles. (d) SEM and EDX elemental mapping images of Fe, Ni, and S for $Fe_{11.8\%}$-Ni_3S_2 Ni_3S_2/NF. XPS spectra in (e) Ni 2p and (f) Fe 2p regions for $Fe_{11.8\%}$-Ni_3S_2/NF.

The electrochemical OER performance of $Fe_{11.8\%}$-Ni_3S_2/NF electrode was first evaluated in O_2-saturated 1 M KOH with a scan rate of 2 mV/s, using a standard three-electrode system. For comparison, blank NF, Ni_3S_2/NF, and RuO_2 on NF (RuO_2/NF) electrodes were also examined. All potentials were reported with respect to RHE (reversible hydrogen electrode) and an *iR* compensation was applied to all initial data for further analysis because as-measured reaction currents cannot directly reflect the intrinsic behavior of catalysts due to the effect of ohmic resistance.[38] Fig. 2a presents the polarization curves. The oxidation peaks at ~1.4 V vs. RHE are attributed to the formation of Ni(III).[13,30] As observed, RuO_2/NF is highly active for OER with 100 mA/cm^2 at overpotential of 257 mV while blank NF has negligible OER activity. Ni_3S_2/NF is also active for OER with the need of overpotential of 431 mV to drive 100 mA/cm^2. It is surprising to find that $Fe_{11.8\%}$-Ni_3S_2/NF has significantly enhanced catalytic activity requiring much lower overpotential of only 253 mV to afford 100 mA/cm^2. This current density compares favorably to the behavior of many recent non-noble metal OER catalysts at the same overpotential, including FeNi-GO/LDH (50 mA/cm^2),[39] H-LDH-1 (~72 mA/cm^2),[40] NiFe/NF (~32 mA/cm^2),[30] CQDs/NiFe-LDH (~22 mA/cm^2),[41] $NiFeO_x$/CFP (~28 mA/cm^2),[42] NiFe-LDH/CNT on CFP (~23 mA/cm^2),[19] $Ni_{2/3}Fe_{1/3}$-GO (~20 mA/cm^2),[43] NiFe LDH/NF (~13 mA/cm^2),[22] and NiFe NS (~2 mA/cm^2),[44] etc. At the same overpotential, the current density of $Fe_{11.8\%}$-Ni_3S_2/NF based on the loading mass is 12.7 mA/mg (Fig. S4). Although it is lower than that of $NiFeO_x$/CFP (~17.5 mA/mg)[42] and NiFe NS (~28.6 mA/mg),[44] it is higher than that of NiFe-LDH (~8.9 mA/mg),[41] $Ni_{2/3}Fe_{1/3}$-NS (~12.1 mA/mg),[43] NiFe (~3.6 mA/mg),[45] and Fe-Ni-O_x-MPs (~8.9 mA/mg).[46] To estimate the effective surface areas of $Fe_{11.8\%}$-Ni_3S_2/NF and Ni_3S_2/NF, we measured the capacitances of the double layer at the solid-liquid interface of both electrodes.[47] The cyclic voltammograms (CVs) were collected in the region of 1.07-1.17 V in 1 M KOH, where the current response should be only due to the charging of the double layer (Fig. S5). The capacitances of $Fe_{11.8\%}$-Ni_3S_2/NF and Ni_3S_2/NF are 14.6 and 6.5 mF/cm^2, respectively, demonstrating $Fe_{11.8\%}$-Ni_3S_2/NF has much higher surface roughness than Ni_3S_2/NF. Thus, the superior OER activity of $Fe_{11.8\%}$-Ni_3S_2/NF can be partially associated with the high surface area.[48] Previous reports demonstrated that the introduction of Fe into the Ni-based nanostructured material can promote the formation and stabilization of the catalytically active species, leading to high OER performance.[49]

The catalytic kinetics for these OER electrodes was further examined by Tafel plots (Fig. 2b). The $Fe_{11.8\%}$-Ni_3S_2/NF exhibits lower Tafel slope (65.5 mV/dec) than Ni_3S_2/NF (107.1 mV/dec), implying Fe doping gives faster OER kinetic and higher performance. The multi-step chronopotentiometric curve (Fig. 2c) shows that at the start of 100 mA/cm^2 the potential immediately levels off at 1.54 V and remains constant for the rest 500 s. All current densities tested up to 600 mA/cm^2 give similar results, showing the excellent mass transport property, conductivity, and mechanical robustness of this $Fe_{11.8\%}$-Ni_3S_2/NF electrode. Because long-term stability is another critical parameter determining the practical ability of an electrocatalyst, we probed the stability of $Fe_{11.8\%}$-Ni_3S_2/NF by chronopotentiometric test. As shown in Fig. 2d, this electrode preserves its catalytic activity for at least 14 h, confirming its strong electrochemical stability. Fig. 2e and 2f show the XPS spectra in Ni 2p and Fe 2p regions of $Fe_{11.8\%}$-Ni_3S_2/NF after OER electrolysis, respectively. As shown in Fig. 2e, the peaks corresponded to Ni $2p_{3/2}$ and Ni $2p_{1/2}$ and their satellite peaks

are still preserved in the Ni 2p region. The peak at 858.1 eV reveals the occurrence NiOOH.[50] The formation of NiOOH is also confirmed by the additional peak at 533.5 eV in the O 1s region (Figure S6b),[50] with the increased peak intensity of Ni-O-S in the S 2p region (Fig. S6a). The The XPS spectrum in Fe 2p region (Fig. 2f) shows two peaks at 711.4 and 724.9 eV and two satellite peaks around 718.9 and 733.1 eV, confirming the formation of FeOOH.[51] The formation of NiOOH and FeOOH was also confirmed by the Raman spectra (Fig. S7). After OER catalysis there are only three peaks, the peak around 305 cm^{-1} attributes to FeOOH[52] and the other two belong to NiOOH.[53] These observations conclude the evolution of NiOOH and FeOOH species at the electrode surface as the active phases for OER.[54,55]

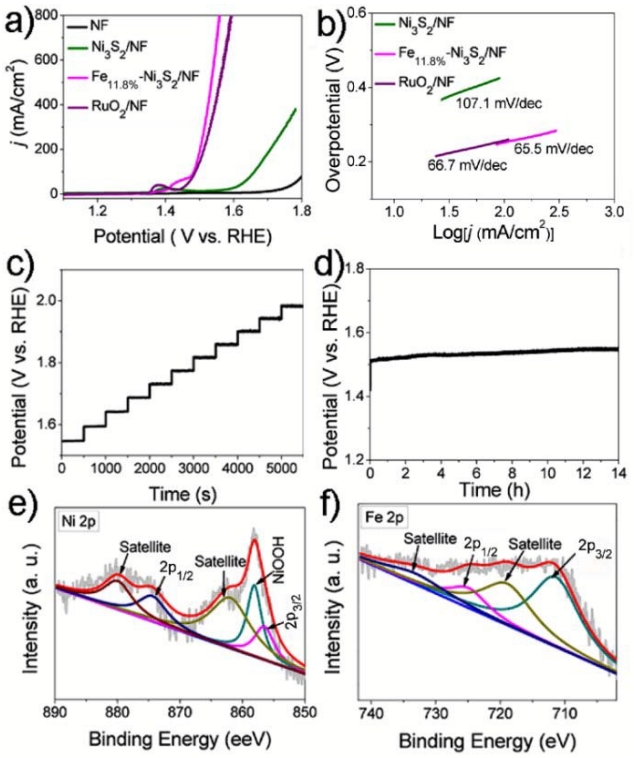

Fig. 2 (a) Polarization curves for blank NF, Ni_3S_2/NF, $Fe_{11.8\%}$-Ni_3S_2/NF, and RuO_2/NF with a scan rate of 2 mV/s. (b) Tafel plots for Ni_3S_2/NF, $Fe_{11.8\%}$-Ni_3S_2/NF, and RuO_2/NF. (c) Multi-current process of $Fe_{11.8\%}$-Ni_3S_2/NF. The current density started at 100 mA/cm^2 and ended at 600 mA/cm^2, with an increment of 50 mA/cm^2 per 500 s without *iR* correction. (d) Chronopotentiometric curve of $Fe_{11.8\%}$-Ni_3S_2/NF with constant current density of 200 mA/cm^2. XPS spectra in (e) Ni 2p region and (f) Fe 2p regions of $Fe_{11.8\%}$-Ni_3S_2/NF after OER electrolysis. The electrolyte is 1 M KOH.

Because practical water electrolysis usually operates in a 25-30 wt% KOH,[56] we further tested the OER performance of the $Fe_{11.8\%}$-Ni_3S_2/NF electrode in 30 wt% KOH. This electrode exhibits larger current densities and lower Tafel slope (64.3 mV/dec) compared with those in 1 M KOH, as shown in Fig. 3a and 3b. The oxidation peaks shift to ~1.25 V vs. RHE, which is consistent with previous report that the oxidation peak potential would shift to less anodic potential value with increased basic concentration.[57] It needs overpotential of 222 mV to attain 300 mA/cm^2, which is comparable to that for RuO_2/NF (221 mV) but much smaller than those for Ni_3S_2/NF (322 mV) and highly active NiFe/NF (340 mV).[30] Also note that this electrode requires small overpotentials of 238 and 269 mV to drive very high current densities of 500 and 1,000 mA/cm^2, respectively. The observation of small OER activity attenuation of this electrode after 14 h OER electrolysis (Fig. 3c) suggests its strong long-term electrochemical stability even under such strongly basic condition.

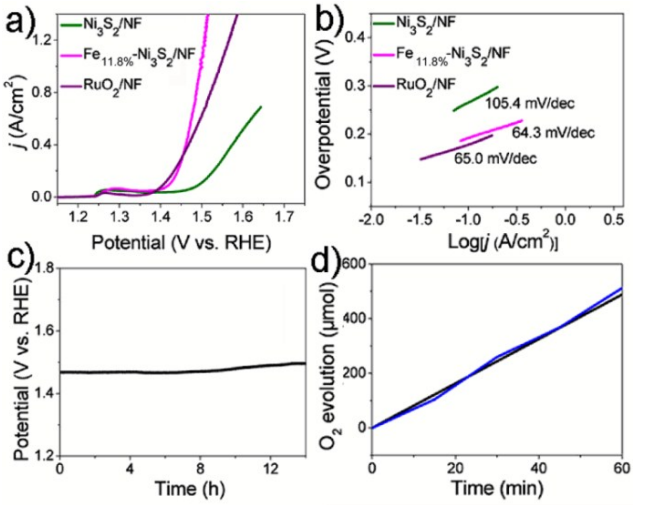

Fig. 3 (a) Polarization curves for Ni_3S_2/NF, $Fe_{11.8\%}$-Ni_3S_2/NF, and RuO_2/NF with a scan rate of 2 mV/s. (b) Tafel plots for Ni_3S_2/NF, $Fe_{11.8\%}$-Ni_3S_2/NF, and RuO_2/NF. (c) Chronopotentiometric curve of $Fe_{11.8\%}$- Ni_3S_2/NF with constant current density of 500 mA/cm^2. (d) The amount of O_2 theoretically calculated (black curve) and experimentally measured (blue curve) versus time for $Fe_{11.8\%}$-Ni_3S_2/NF at 1.6 V for 60 min. All experiments were carried out in 30 wt% KOH.

The evolved O_2 was confirmed by gas chromatography (GC) analysis and its total amount (n) was measured quantitatively using a calibrated pressure sensor to monitor the pressure change in the anode compartment of a H-type electrolytic cell according to established method.[38,58] Potentiostatic electrolysis was performed at 1.6 V for 60 min. The FE of $Fe_{11.8\%}$-Ni_3S_2/NF for oxygen evolution was determined by comparing the amount of generated O_2 with theoretically calculated value (assuming 100% FE). The total amount of charge (Q) passed through the cell was obtained from the current-time curve and the FE can be calculated from FE = n/(Q/4F), where F is the Faraday constant. The agreement of both values suggests 100% FE (Fig. 3d), implying the current density is directly related to oxygen evolution.

We further examined the effect of Fe-content on the OER activity by preparing another two samples with Fe-content of 6.5% ($Fe_{6.5\%}$-Ni_3S_2/NF) and 14.9% ($Fe_{14.9\%}$-Ni_3S_2/NF). Although no obvious differences in structure and morphology are observed for three samples (Fig. S8), both $Fe_{6.5\%}$-Ni_3S_2/NF and $Fe_{14.9\%}$-Ni_3S_2/NF electrodes exhibit inferior OER activity over $Fe_{11.8\%}$-Ni_3S_2/NF in 30 wt% KOH requiring overpotentials of 261 and 280 mV to drive 300 mA/cm^2, respectively (Fig. 4a). Fig. 4b presents the Tafel plots for $Fe_{6.5\%}$-Ni_3S_2/NF and $Fe_{14.9\%}$-Ni_3S_2/NF, indicating $Fe_{11.8\%}$-Ni_3S_2/NF has smaller Tafel slope and thus more favorable OER kinetic than $Fe_{6.5\%}$-Ni_3S_2/NF (77.1 mV/dec) and $Fe_{14.9\%}$-Ni_3S_2/NF (108.7 mV/dec). To estimate the effective surface areas of the samples, we collected the CVs in

the region of 1.07-1.17 V in 30 wt% KOH (Fig. S9). The capacitances of $Fe_{6.5\%}$-Ni_3S_2/NF, $Fe_{11.8\%}$-Ni_3S_2/NF and $Fe_{14.9\%}$-Ni_3S_2/NF are 15.6, 31.3, and 12.4 mF/cm^2, respectively, demonstrating $Fe_{11.8\%}$-Ni_3S_2/NF has much higher surface roughness than $Fe_{6.5\%}$-Ni_3S_2/NF and $Fe_{14.9\%}$-Ni_3S_2/NF. Thus, the superior OER activity of $Fe_{11.8\%}$-Ni_3S_2/NF can be partially associated with the high surface area.[48] It should be mentioned that the decreased catalytic activity with further increased Fe content can also be partially ascribed to that more Fe would suppress the electrochemical oxidation of Ni(II) to Ni(III) and decrease the number of Ni active sites on the catalytic surface.[36,59]

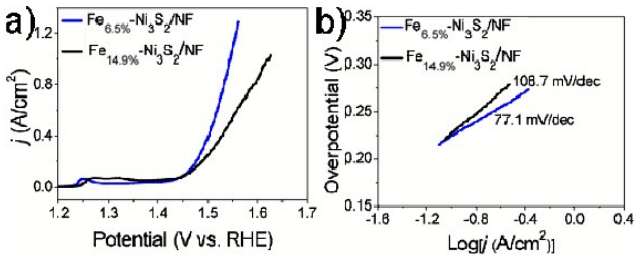

Fig. 4 (a) Polarization curves for $Fe_{6.5\%}$-Ni_3S_2/NF and $Fe_{14.9\%}$-Ni_3S_2/NF with a scan rate of 2 mV/s. (b) The corresponding Tafel plots. All experiments were carried out in 30 wt% KOH.

Conclusions

In summary, Fe-doped Ni_3S_2 particles film with different Fe-content has been hydrothermally developed on nickel film. The $Fe_{11.8\%}$-Ni_3S_2/NF behaves a high-efficiency and robust oxygen evolution electrode with very high current density in strongly alkaline electrolytes. It requires overpotential of only 253 mV to drive 100 mA/cm^2 with its catalytic activity being maintained for at least 14 h in 1 M KOH. In 30 wt% KOH, small overpotentials of 238 mV and 269 mV are needed to attain 500 and 1000 mA/cm^2, respectively. The superior catalytic activity and stability meets the strict criteria for practical industrial uses. We believe that this work not only provides us a low-cost, stable, and active oxygen evolution catalyst, but points out the new direction in designing and developing metal-doped transition metal chalcogenides as attractive heterogeneous catalytic materials toward applications in water-splitting devices and metal-air batteries.[60]

Acknowledgements

This work was supported by the National Natural Science Foundation of China (No. 21175129), the National Basic Research Program of China (No. 2011CB935800), and the "Strategic Priority Research Program" of the Chinese Academy of Sciences (No. XDA09030104).

Notes and references

1. A. J. Bard and M. A. Fox, Acc. *Chem. Res*., 1995, **28**, 141-145.
2. M. D. Symes and L. Cronin, *Nat. Chem.,* 2013, **5**, 403-409.
3. T. R. Cook, D. K. Dogutan, S. Y. Reece, Y. Surendranath, T. S. Teets and D. G. Nocera, *Chem. Rev.,* 2010, **110**, 6474-6502.
4. M. G. Walter, E. L. Warren, J. R. McKone, S. W. Boettcher, Q. Mi, E. A. Santori and N. S. Lewis, *Chem. Rev.,* 2010, **110**, 6446-6473.
5. H. Dau, C. Limberg, T. Reier, M. Risch, S. Roggan and P. Strasser, *ChemCatChem,* 2010, **2**, 724-761.
6. J. O. M. Bockris, *J. Chem. Phys.,* 1956, **24**, 817-827.
7. D. Gust, T. A. Moore and A. L. Moore, *Acc. Chem. Res.,* 2009, **42**, 1890-1898.
8. J. Wang, H. Zhong, Y. Qin and X. Zhang, *Angew. Chem. Int. Ed.,* 2013, **52**, 5248-5253.
9. J. Trotochaud, J. K. Ranney, K. N. Williams and S. W. Boettcher, *J. Am. Chem. Soc.,* 2012, **134**, 17253-17261.
10. M. Gao, W. Sheng, Z. Zhuang, Q. Fang, S. Gu, J. Jiang and Y. Yan, *J. Am. Chem. Soc.,* 2014, **136**, 7077-7084.
11. H. Wang, H.-W. Lee, Y. Deng, Z. Lu, P.-C. Hsu, Y. Liu, D. Lin and Y. Cui, *Nat. commun.,* 2015, ***6***, 7261.
12. W. Zhou, X. Wu, X. Cao, X. Huang, C. Tan, J. Tian, H. Liu, J. Wang and H. Zhang, *Energy Environ. Sci.,* 2013, **6**, 2921-2924.
13. C. Tang, N. Cheng, Z. Pu, W. Xing and X. Sun, *Angew. Chem. Int. Ed*., 2015, **54**, 9351-5354.
14. K. Xu, P. Chen, X. Li, Y. Tong, H. Ding, X. Wu, W. Chu, Z. Peng, C. Wu and Y. Xie, *J. Am. Chem. Soc.,* 2015, **137**, 4119-4125.
15. M. Shalom, D. Ressing, X. Yang, G. Clavel, T. P. Fellinger and M. Antonietti, *J. Mater. Chem. A,* 2015, **3**, 8171-8177.
16. R. D. L. Smith, M. S. Prévot, R. D. Fagan, S. Trudel and C. P. Berlinguette, *J. Am. Chem. Soc*., 2013, **135**, 11580-11586.
17. R. D. L. Smith, M. S. Prevot, R. D. Fagan, Z. Zhang, P. A. Sedach, M. K. J. Siu, S. Trudel and C. P. Berlinguette, *Science,* 2013, **340**, 60-63.
18. Y. Li, P. Hasin and Y. Wu, *Adv. Mater.,* 2010, **22**, 1926-1929.
19. M. Gong, Y. Li, H. Wang, Y. Liang, J. Wu, J. Zhou, J. Wang, T. Regier, F. Wei and H. Dai, *J. Am. Chem. Soc*., 2013, **135**, 8452-8455.
20. S. Chen, J. Duan, M. Jaroniec and S. Qiao, *Angew. Chem. Int. Ed*., 2013, **52**, 13567-13570.
21. X. Long, J. Li, S. Xiao, K. Yan, Z. Wang, H. Chen and S. Yang, *Angew. Chem. Int. Ed.,* 2014, **53**, 7584-7588.
22. J. Luo, J.-H. Im, M. T. Mayer, M. Schreier, M. K. Nazeeruddin, N. G. Park, S. D. Tilley, H. Fan and M. Grätzel, *Science,* 2014, **345**, 1593-1596.
23. L. Kuai, J. Geng, C. Chen, E. Kan, Y. Liu, Q. Wang and B. Geng, *Angew. Chem. Int. Ed.,* 2014, ***53***, 7547-7551.
24. Z. Zhao, H. Wu, H. He, X. Xu and Y. Jin, *J. Mater. Chem. A,* 2015, **3**, 7179-7186.
25. Q. Liu, J. Jin and J. Zhang, *ACS Appl. Mater. Interfaces,* 2013, **5**, 5002-5008.
26. C. Ouyang, X. Wang, C. Wang, X. Zhang, J. Wu, Z. Ma, S. Dou and S. Wang, *Electrochim. Acta*, 2015, **174**, 297-301.
27. D. Friebel, M. W. Louie, M. Bajdich, K. E. Sanwald, Y. Cai, A. M. Wise, M.-J. Cheng, D. Sokaras, T.-C. Weng, R. Alonso-Mori, R. C. Davis, J. R. Bargar, J. K. Nørskov, A. Nilsson and A. T. Bell, *J. Am. Chem. Soc*., 2015, **137**, 1305-1313.
28. Y. Zhang, X. Cao, H. Yuan, W. Zhang and Z. Zhou, *Int. J. Hydrogen Energy,* 1999, **24**, 529-536.
29. L. Trotochaud, S. L. Young, J. K. Ranney and S. W. Boettcher, *J. Am. Chem. Soc.,* 2014, **136**, 6744-6753.
30. X. Lu and C. Zhao, *Nat. Commun.,* 2015, **6**, 6616.
31. Y. Tang, T. Chen and S. Yu, *Chem. Commun.,* 2015, **51**, 9018-9021.
32. B. Zhang, X. Ye, W. Dai, W. Hou and Y. Xie, *Chem. Eur. J.*, 2006, **12**, 2337-2342.
33. M. C. Biesinger, B. P. Payne, L. W. M. Lau, A. Gerson and R. St. C. Smart, *Surf. Interface Anal.,* 2009, **41**, 324-332.
34. X. Liu, J. Liu and X. Sun, *J. Mater, Chem. A,* 2015, **3**, 13900-13905.

35. Y. W. Zhu, T. Yu, C. H. Sow, Y. J. Liu, A. T. S. Wee, X. J. Xu and C. T. Lim, *Appl. Phys. Lett.,* 2005, **87**, 023103.
36. K. Fominykh, P. Chernev, I. Zaharieva, J. Sicklinger, G. Stefanic, M. Döblinger, A. Müller, A. Pokharel, S. Böcklein, C. Scheu, T. Bein and D. Fattakhova-Rohlfing, *ACS Nano,* 2015, **9**, 5180-5188.
37. C. Dueso, M. T. Izquierdo, F. García-Labiano, L. F. de Diego, A. Abad, P. Gayán and J. Adánez, *Appl. Catal. B,* 2012, **126**, 186-199.
38. Z. Xing, Q. Liu, A. M. Asiri and X. Sun, *Adv. Mater.,* 2014, **26**, 5702-5707.
39. X. Long, J. Li, S. Xiao, K. Yan, Z. Wang, H. Chen and S. Yang, *Angew. Chem. Int. Ed.,* 2014, **53**, 7584-7588.
40. Q. Yang, T. Li, Z. Lu, X. Sun and J. Liu, *Nanoscale,* 2014, **6**, 11789-11794.
41. D. Tang, J. Liu, X. Wu, R. Liu, X. Han, Y. Han, H. Huang, Y. Liu and Z. Kang, *ACS Appl. Mater. Interfaces,* 2014, **6**, 7918-7925.
42. H. Wang, H.-W. Lee, Y. Deng, Z. Lu, P.-C. Hsu, Y. Liu, D. Lin and Y. Cui, *Nat. commun.*, 2015, **6**, 7261.
43. W. Ma, R. Ma, C. Wang, J. Liang, X. Liu, K. Zhou and T. Sasaki, *ACS Nano,* 2015, **9**, 1977-1984.
44. F. Song and X. Hu, *Nat. Commun.,* 2014, **5**, 4477.
45. N. Han, F. Zhao and Y. Li, *J. Mater. Chem. A,* 2015, **3**, 16348-16353.
46. L. Wang, J. Geng, W. Wang, C. Yuan, L. Kuai and B. Geng, *Nano Res*., DOI: 10.1007/S12274-015-0881-0.
47. S. Trasatti and O. A. Petrii, *J. Electroanal. Chem.,* 1992, **327**, 353-376.
48. J. Tian, Q. Liu, N. Cheng, A. M. Asiri and X. Sun, *Angew. Chem. Int. Ed.,* 2014, **53**, 9577-9581.
49. Z. Zhao, H. Wu, H. He, X. Xu and Y. Jin, *J. Mater. Chem. A* 2015, **3**, 7179-7186.
50. M. S. Hamdan, Riyanto and M. R. Othman, *Int. J. Elelectrochem. Sci.,* 2013, **8**, 4747-4760.
51. C. Long, L. Jiang, T. Wei, J. Yan and Z. Fan, *J. Mater. Chem. A,* 2014, **2**, 16678-16686.
52. M. Pradhan, S. Maji, A. K. Sinha, S. Dutta and T. Pal, *J. Mater. Chem. A*, 2015, **3**, 10254-10257.
53. K. S. Joya and X. Sala, *Phys. Chem. Chem. Phys*., 2015, **17**, 21094-21103.
54. M. W. Louie and A. T. Bell, *J. Am. Chem. Soc.,* 2013, **135**, 12329-12337.
55. M. E. G. Lyons and M. P. Brandon, *Phys. Chem. Chem. Phys.,* 2009, **11**, 2203-2217.
56. K. Mazloomi, N. b. Sulaiman and H. Moayedi, *Int. J. Electrochem. Sci.,* 2012, **7**, 3314-3326.
57. M. E. G. Lyons, L. Russell, M. O'Brien, R. L. Doyle, I. Godwin and M. P. Brandon, *Int. J. Electrochem. Sci*., 2012, **7**, 2710-2763.
58. J. Tian, Q. Liu, A. M. Asiri and X. Sun, *J. Am. Chem. Soc.,* 2014, **136**, 7587-7590.
59. Y. Qiu, L. Xu and W. Li, *Langmuir*, 2014, **30**, 7893-7901.
60. F. Cheng and J. Chen, *Chem. Soc. Rev.,* 2012, **41**, 2172-2192.